Electronic Supplementary Material (ESI) for Physical Chemistry Chemical Physics.

Electronic Supplementary Information

Highly sensitive gating in pH-responsive nanochannels as a result of ionic bridging and nanoconfinement

Luis G. Lopez*, Rikkert J. Nap

Department of Biomedical Engineering, Department of Chemistry, and Chemistry of Life Processes Institute, Northwestern University, Evanston, Illinois 60208, United States.

* luis.lopez@northwestern.edu.

Free energy functional.

The free energy functional (per unit area) that determines the equilibrium state of the system is given by

$$\begin{aligned}\frac{\beta F}{A(R)} = {} & \frac{N_P}{A(R)}\sum_{\alpha} P_P(\alpha)\ln P_P(\alpha) + \sum_i \int_0^R drG(r)\rho_i(r)(\ln \rho_i(r)v_w - 1) + \beta\sum_i \mu_i^0 \int_0^R drG(r)\rho_i(r) \\ & + \int_0^R drG(r)\langle\rho_P(r)\rangle\Big\{f_{A^-}(r)\left[\ln f_{A^-}(r) + \beta\mu_{A^-}^0\right] + f_{AH}(r)\left[\ln f_{AH}(r) + \beta\mu_{AH}^0\right] \\ & + f_{ANa}(r)\left[\ln f_{ANa}(r) + \beta\mu_{ANa}^0\right] + f_{ACa^+}(r)\left[\ln f_{ACa^+}(r) + \beta\mu_{Aca^+}^0\right] \\ & + \frac{1}{2}f_{A_2Ca}(r)\left[\ln\frac{f_{A_2Ca}(r)}{2} + \beta\mu_{A_2Ca}^0 - \left(\ln\langle\rho_P(r)\rangle v_w - 1\right)\right]\Big\} \\ & + \beta\int_0^R drG(r)\left[\langle\rho_q(r)\rangle\psi(r) - \frac{1}{2}\varepsilon_0\varepsilon_w(\nabla_r\psi(\mathrm{r}))^2\right] \\ & + \frac{\beta\chi A(R)}{2}\int_0^R\int_0^R drdr'G(r)G(r')\langle\rho_P(r)\rangle g(r,r')\langle\rho_P(r')\rangle \\ & + \beta\int_0^R drG(r)\pi(r)\left(\langle\phi_P(r)\rangle + \sum_i \phi_i(r) - 1\right)\end{aligned} \tag{1}$$

Each of the terms in eq. (1) is described in the theory section of the main text. Thus, the free energy functional is composed of the abovementioned six terms, which, starting with the term corresponding to the conformational entropy of the polymers, are defined per unit area as follows

$$-\frac{S_{conf}}{k_B A(R)} = \frac{N_P}{A(R)}\sum_{\alpha} P_P(\alpha)\ln P_P(\alpha) \tag{2}$$

where $P_P(\alpha)$ is the probability of finding an end-tethered polymer chain in the conformation α. Each conformation is defined by the position of all the polymer segments belonging to a chain. It is worth mentioning, that the probability distribution function (pdf) constitutes a fundamental quantity in our formulation, since all thermodynamic and structural properties can be calculated from it. In particular, the average number density of polymers at the position r, which is given by

$\langle\rho_P\rangle = \frac{\sigma_P}{G(r)}\sum_\alpha P(\alpha)n(\alpha;r)$. Where $n_p(\alpha;r)$ is the number of polymer segments at r (when the polymer is in the conformation α), and the function $G(r) = A(r)/A(R) = r/R$ is a geometrical factor that considers the volume changes with r.[1]

The translational entropy of the mobile species is represented by

$$-\frac{S_{trans}}{k_B A(R)} = \sum_i \int_0^R drG(r)\rho_i(r)(\ln \rho_i(r)v_w - 1) \tag{3}$$

where the index i runs over all the different types of mobile species (i = Na^+, Cl^-, Ca^{2+}, H^+, OH^-, and water, which is symbolized by w), $\rho_i(r)$ is the number density of the species i at r, and v_w is the volume of a water molecule.

The third term, F_{chem}, takes into account the entropic and enthalpic contributions of all possible states of each acidic group: protonated (AH), deprotonated (A^-), sodium bound (ANa), and calcium bound (ACa^+), as well as the formation of inter and intramolecular calcium bridges (A_2Ca), as follows

$$\begin{aligned}\frac{\beta F_{chem}}{A(R)} &= \beta\sum_i \int_0^R drG(r)\rho_i(r)\,\mu_i^0 \\ &+ \int_0^R drG(r)\langle\rho_P(r)\rangle\Big\{f_{A^-}(r)[\ln f_{A^-}(r) + \beta\mu_{A^-}^0] + f_{AH}(r)[\ln f_{AH}(r) + \beta\mu_{AH}^0] \\ &+ f_{ANa}(r)[\ln f_{ANa}(r) + \beta\mu_{ANa}^0] + f_{ACa^+}(r)\big[\ln f_{ACa^+}(r) + \beta\mu_{Aca^+}^0\big] \\ &+ \frac{1}{2}f_{A_2Ca}(r)\left[\ln\frac{f_{A_2Ca}(r)}{2} + \beta\mu_{A_2Ca}^0 - (\ln\langle\rho_P(r)\rangle v_w - 1)\right]\Big\}\end{aligned} \tag{4}$$

where $\beta = 1/k_BT$, the index i runs over all the mobile species (i = Na^+, Cl^-, Ca^{2+}, H^+, and OH^-), and μ_i^0 is the corresponding standard chemical potential. $\langle\rho_P(r)\rangle$ is the average number density of polymer segments at r (as previously mentioned), and $f_j(r)$ is the fraction of polymer segments in state j at r (j = A^-, AH, ANa, ACa^+, A_2Ca). The total number density of monomers is conserved: $\sum_j f_j\,(r) = 1$. The standard chemical potentials, μ_i^0 and μ_j^0, describing the standard free energy

associated with the formation of the mobile species *i* and polymer segments in state *j*, respectively, can be related to the equilibrium dissociation constants of an isolated group in the bulk (see Table 1, Main Text) by $K_d = C \exp[-\beta(\mu_{A^-}^0 + \mu_X^0 - \mu_{AX}^0)]$; where *C* is a constant ($C = 1/N_A v_w$), and *X* and *AX* respectively represent H^+, Na^+, or Ca^{2+} and the corresponding complex: AH, ANa, or ACa^+, as applicable. In the case of the A_2Ca complex, $K_{A_2Ca} = C' \exp[-\beta(2\mu_{A^-}^0 + \mu_{Ca^{2+}}^0 - \mu_{A_2Ca}^0)]$ (where $C' = C^2$). When calculating the thermodynamic contributions of each A_2Ca complex, two aspects must be considered. First, since the total number density of A_2Ca complexes is half of the number density of acidic segments participating in a calcium bridge (A_2Ca), a factor of ½ has to be introduced to properly count the number of acidic monomers involved. Second, the term $\frac{1}{2} f_{A_2Ca}(r)(\ln\langle\rho_P(r)\rangle v_w - 1)$ takes into account the loss of entropy that occurs when two acidic segments get combined into one A_2Ca complex. Higher-order complexes[2] between Ca^{2+} and PAA segments have not been considered in this approximation. A detailed derivation is presented in Ref.[3]

The term corresponding to the total electrostatic energy is defined as

$$\frac{\beta F_{elect}}{A(R)} = \beta \int_0^R dr G(r) \left[\langle \rho_q(r) \rangle \psi(r) - \frac{1}{2} \varepsilon_0 \varepsilon_w (\nabla_r \psi(\mathrm{r}))^2 \right] \quad (5)$$

where $\psi(\mathrm{r})$ is the local electrostatic potential; $\nabla_r \psi(\mathrm{r})$ is the gradient in the radial direction; ε_0 is the dielectric permittivity of vacuum and ε_w is the relative dielectric constant of the aqueous solution ($\varepsilon_w = 78.5$); and $\langle \rho_q(r) \rangle$ is the average charge density at *r*, which is given by $\langle \rho_q(r) \rangle = \sum_k e z_k \rho_k(r) - e\langle \rho_P(r) \rangle (f_{A^-}(r) - f_{ACa^+}(r))$. Regarding the expression for $\langle \rho_q(r) \rangle$, the summation in the first term runs over all charged mobile species *k* (*k* = Na^+, Cl^-, Ca^{2+}, H^+, and OH^-), with z_k being the corresponding valence and *e* the unit of charge. The second term, takes into account the charge contribution of all charged segments (A^- and ACa^+).

The fifth term of the free energy expression, which describes the effective attractive interactions between segments, is defined by

$$\frac{\beta E_{vdW}}{A(R)} = \frac{\beta\chi A(R)}{2}\int_0^R\int_0^R drdr'G(r)G(r')\langle\rho_P(r)\rangle g(r,r')\,\langle\rho_P(r')\rangle \tag{6}$$

where χ represents the segment-segment interaction strength and the function $g(r,r')$ models the distance dependence of the attraction between a segment at r and a segment at r'. The complete expression constitutes a direct way to describe the effects of solvent quality on the distribution of polymer conformations.[4] In our calculations, we assumed good solvent conditions ($\chi = 0$). This simplification is validated by the fact that the quality of the solvent has shown to have an insignificant effect on the conductance curves predicted for a P4VP-functionalized nanochannel, where different segment-segment hydrophobic interaction strengths have been evaluated.[5] It is worth mentioning here, that the formation of hydrogen bounds has not be considered in this formulation. This aspect, together with the assumption of good solvent conditions, implies that the only way for the polymers to collapse is through electrostatic interactions between charged segments and counterions. Finally, the last term of the free energy equation takes into account the repulsive interactions present in the system and is given by

$$\frac{\beta E_{rep}}{A(R)} = \beta\int_0^R drG(r)\pi(r)\left(\langle\phi_P(r)\rangle + \sum_i \phi_i(r) - 1\right) \tag{7}$$

Here, the intermolecular repulsions are modeled as excluded volume interactions, assuming incompressibility in the system at every point. $\pi(r)$ are the Lagrange multipliers that enforce the local packing constraints (excluded volume interactions), and correspond to the local osmotic pressures.[1] $\langle\phi_p(r)\rangle$ is the polymer volume fraction, which is equal to $\langle\rho_P(r)\rangle\sum_j f_j(r)v_j$, where $f_j(r)$ is the fraction of polymer segments in state j at r (j = A^-, AH, ANa, ACa^+, A_2Ca), and v_j is its

corresponding volume. Similarly, $\phi_i(r)$ is the volume fraction of the free species i, and is equal to the term $\rho_i(r)v_i$.

The equilibrium state of the system can be found by minimizing the free energy functional with respect to: $P_P(\alpha)$, $\rho_i(r)$, $f_{AX}(r)$ and $f_{A_2Ca}(r)$, and varied with respect to the electrostatic potential, $\psi(r)$ (see next section). The procedure results in a system of non-linear coupled integro-differential equations that can be discretized in the r direction and solved by standard numerical methods.[1, 6] In order to solve these equations, the following inputs must be specified: σ, R, bulk pH, C_{NaCl} and C_{CaCl2} in the bulk solution, the dissociation equilibrium constants of AX and A_2Ca (Table 1, Main Text), and a set of unbiased chain conformations. All the results presented in this paper have been calculated for R = 7.5 nm, the pK_d's of Table 1 (Main Text), and a set of 2 x 10^6 chain conformations generated with the rotational isomeric state (RIS) model. The probability of each conformation, $P_P(\alpha)$, is weighted by the theory. The molecular theory provides π(r), $\rho_i(r)$, $\psi(r)$, $f_{AX}(r)$ and $f_{A_2Ca}(r)$ as output, as well as thermodynamic and structural quantities of interest.

Free energy functional minimization.

The minimization of the free energy functional is subject to the packing constraint and the global electroneutrality condition, which are defined respectively as follows

$$\langle \phi_P(r) \rangle + \sum_i \rho_i(r) v_i = 1 \tag{8}$$

$$\int_0^R \langle \rho_q(r) \rangle \, r dr = 0 \tag{9}$$

Where i runs over all the mobile species (i = Na^+, Cl^-, Ca^{2+}, H^+, OH^-, and water). The averages of the polymer volume fraction, $\langle\phi_P(r)\rangle$, and the density of charges, $\langle\rho_q(r)\rangle$, at r, were defined in the previous section.

The system is in contact with the bulk solution, which contains water, anions, cations, protons and hydroxyl ions (with their chemical potential being constant at every point in the system at equilibrium). Hence, the proper thermodynamic potential is the semi-grand potential given by

$$\begin{aligned}\frac{\beta W}{A(R)} = \frac{\beta F}{A(R)} - \sum_{k=\{w,Cl^-,OH^-\}} \beta\mu_k \int_0^R drG(r)\rho_k(r) - \beta\mu_{H^+}\int_0^R drG(r)(\rho_{H^+}(r) + f_{AH}(r)\langle\rho_P(r)\rangle) \\ - \beta\mu_{Na^+}\int_0^R drG(r)(\rho_{Na^+}(r) + f_{ANa}(r)\langle\rho_P(r)\rangle) \\ - \beta\mu_{Ca^{2+}}\int_0^R drG(r)\left(\rho_{Ca^{2+}}(r) + \left(f_{ACa^+}(r) + \frac{1}{2}f_{A_2Ca}(r)\right)\langle\rho_P(r)\rangle\right) \\ + \beta\int_0^R drG(r)\lambda(r)\langle\rho_P(r)\rangle\left(f_{A^-}(r) + f_{AH}(r) + f_{ANa}(r) + f_{ACa^+}(r) + f_{A_2Ca}(r)\right) - 1) \\ + \beta\int_0^R drG(r)\pi(r)\left(\langle\phi_P(r)\rangle + \sum_k \rho_k(r)v_k - 1\right) + \beta\lambda_{en}\int_0^R drG(r)\,\rho_q(r)\end{aligned} \tag{10}$$

here $\pi(r)$, $\lambda(r)$, and λ_{en} are the Lagrange multipliers introduced to enforce the packing constraint (8), $\sum_j f_j(r) = 1$, and the electroneutrality condition (9), respectively. For protons, sodium and calcium ions, eq. (10) includes the additional contributions coming from the condensed states: AH, ANa, ACa^+, and A_2Ca.

The minimization of eq. (10) with respect to the different polymer segment states ($f_{A^-}(r), f_{AH}(r), f_{ANa}(r), f_{ACa^+}(r)$, and $f_{A_2Ca}(r)$, respectively) results in the following five equivalent expressions of the Lagrange multiplier $\lambda(r)$:

$$\ln f_{A^-}(r) + 1 + \beta\mu^0_{A^-} + \beta\pi(r)v_{A^-} + \beta\psi(r)z_{A^-}e + \beta\lambda(r) = 0 \tag{11}$$

$$\ln f_{AH}(r) + 1 + \beta\mu^0_{AH} - \beta\mu_{H^+} + \beta\pi(r)v_{AH} + \beta\lambda(r) = 0 \quad (12)$$

$$\ln f_{ANa}(r) + 1 + \beta\mu^0_{ANa} - \beta\mu_{Na^+} + \beta\pi(r)v_{ANa} + \beta\lambda(r) = 0 \quad (13)$$

$$\ln f_{ACa^+}(r) + 1 + \beta\mu^0_{ACa^+} - \beta\mu_{Ca^{2+}} + \beta\pi(r)v_{ACa^+} + \beta\psi(r)z_{ACa^+}e + \beta\lambda(r) = 0 \quad (14)$$

$$\frac{1}{2}\left(\ln\frac{f_{A_2Ca}(r)}{2} + \beta\mu^0_{A_2Ca} - \beta\mu_{Ca^{2+}} + \beta\pi(r)v_{A_2Ca} - \ln\langle\rho_P(r)\rangle v_w\right) + 1 + \beta\lambda(r) = 0 \quad (15)$$

The minimization with respect to $P_P(\alpha)$ leads to

$$P_P(\alpha) = \frac{1}{\xi} exp\left(\int_0^R dr\, n_p(\alpha; r)(1 + \beta\lambda(r))\right) \quad (16)$$

where the partition function ξ acts as a normalization constant that ensures the condition $\sum_\alpha P_P(\alpha) = 1$, and $n_p(\alpha; r)dr$ is the number of polymer segments within the volume element [r, r + dr]. Using any of the five equivalent expressions for $\lambda(r)$ (equations (11-15)), $P_P(\alpha)$ can be express in terms of $\pi(r)$ (which is a position-dependent osmotic pressure) and the electrostatic potential, $\psi(r)$. If eq. 11 is used, the following expression is obtained

$$P_P(\alpha) = \frac{1}{\xi} exp\left(-\int_0^R dr\, n_p(\alpha; r)(\beta\pi(r)v_{A^-} + \beta\psi(r)z_{A^-}e + \ln f_{A^-}(r) + \beta\mu^0_{A^-})\right) \quad (17)$$

When eq. (10) is minimized with respect to $\rho_w(r)$ and $\rho_\gamma(r)$ (with $\gamma = Cl^-, OH^-, H^+, Na^+$, or Ca^{2+}) the following expressions for the local density of water and ions, respectively, are obtained,

$$\rho_w(r) = \frac{1}{v_w} exp(-\beta\pi(r)v_w) \quad (18)$$

$$\rho_\gamma(r) = \frac{1}{v_w} exp\left(\beta\mu_\gamma - \beta\mu^0_\gamma - \beta\pi(r)v_\gamma - \beta\psi(r)z_\gamma e\right) \quad (19)$$

The corresponding local volume fractions are: $\phi_w(r) = \rho_w(r)v_w$ for water, and $\phi_\gamma(r) = \rho_\gamma(r)v_\gamma$ for the ions.

The elimination of the Lagrange multiplier λ(r), from the pair of equations (11,12), (11,13), (11,14), and (11,15) leads to a set of equations that govern the chemical equilibrium, namely

$$\frac{f_{A^-}(r)}{f_{AH}(r)} = K^0_{AH}\frac{e^{-\beta\pi(r)\Delta v_{AH}}}{\rho_{H^+}(r)v_w} \tag{20}$$

$$\frac{f_{A^-}(r)}{f_{ANa}(r)} = K^0_{ANa}\frac{e^{-\beta\pi(r)\Delta v_{ANa}}}{\rho_{Na^+}(r)v_w} \tag{21}$$

$$\frac{f_{A^-}(r)}{f_{ACa^+}(r)} = K^0_{ACa^+}\frac{e^{-\beta\pi(r)\Delta v_{ACa^+}}}{\rho_{Ca^{2+}}(r)v_w} \tag{22}$$

$$\frac{f_{A^-}(r)^2\langle\rho_P(r)\rangle v_w}{\frac{1}{2}f_{A_2Ca}(r)} = K^0_{A_2Ca}\frac{e^{-\beta\pi(r)\Delta v_{A_2Ca}}}{\rho_{Ca^{2+}}(r)v_w} \tag{23}$$

Where $K^0_{AX} = \exp(-\beta\Delta G^0_{AX})$ is the chemical equilibrium constant and $\Delta G^0_{AX} = \mu^0_{A^-} + \mu^0_X - \mu^0_{AX}$ is the standard free energy change of the corresponding reactions (as the notation applied in the previous section, see explanation of eq. (4), *X* and *AX* respectively represent H^+, Na^+, or Ca^{2+}, and the corresponding complex: AH, ANa, or ACa^+, as applicable). On the other hand, $\Delta v_{AX} = v_{A^-} + v_X - v_{AX}$ is the difference in volume between products and reactants. For the reaction of one calcium ion with two deprotonated acid groups: $K^0_{A_2Ca} = \exp(-\beta\Delta G^0_{A_2Ca})$, $\Delta G^0_{A_2Ca} = 2\mu^0_{A^-} + \mu^0_{Ca^{2+}} - \mu^0_{A_2Ca}$, and $\Delta v_{A_2Ca} = 2v_{A^-} + v_{Ca^{2+}} - v_{A_2Ca}$.

Finally, the extremum of W (eq. (10)) with respect to the electrostatic potential, ψ(r), gives rise to the Poisson equation

$$\varepsilon_0\varepsilon_w\nabla^2_r\psi(r) = -\langle\rho_P(r)\rangle \tag{24}$$

At *r = 0* and *r = R*, the boundary conditions for eq. (24) are, respectively

$$\left.\frac{\partial\psi(r)}{\partial r}\right|_{r=0} = 0 \tag{25}$$

$$\left.\frac{\partial\psi(r)}{\partial r}\right|_{r=R} = 0 \tag{26}$$

Molecular details.

The molecular details of the ions and molecules that form part of the system under study are listed Table S1. Since a complete dissociation for NaCl and $CaCl_2$ was assumed, the ion pairs are inexistent in the system and a C_{NaCl} = 100 mM (for instance) must be read as 100 mM of Na^+ ions and 100 mM of Cl^- ions in the bulk solution (same for $CaCl_2$, mutatis mutandis). The diffusion coefficient values, used to calculate the conductance of the channel, were taken from Ref.[7] For the acid base equilibrium reaction, a volume variation of v_w is considered. Volume variations for the ion condensation reactions are neglected. Regarding the polymer chain, a three-state rotational isomeric state (RIS) model was used. A set of $2x10^6$ conformations is generated by a Monte Carlo sampling procedure (where segment-segment and segment-wall overlaps are forbidden), and such a set is used for all the calculations reported in the present paper.

	Electrostatic charge, q_i	Molecular volume, v_i (nm^3)	Diffusion coefficient, D_i (m^2/s)
Water	0	0.03	-
H^+	+1	0.03	9.31×10^{-9}
OH^-	-1	0.03	5.28×10^{-9}
Na^+	+1	0.0044	1.33×10^{-9}
Cl^-	-1	0.025	2.03×10^{-9}
Ca^{2+}	+2	0.005	0.79×10^{-9}
Polymer (AA) segment	-1 ($pK_d^{bulk} = 5.0$)	0.07448	-

Table S1. Molecular information of all the species present in the system.

Determination of the dissociation constant values (pK) for AH, ANa, ACa^+, and A_2Ca.

The values presented in Table 1 (see Theoretical Methodology section of the Main Text) were obtained combining experimental data with new and previous simulation results. The pK value for the carboxylic acid group in solution is experimentally well known.[8] However, the chemical equilibrium constants corresponding to the condensation of carboxylate groups with different cations have been more difficult to establish. This is particularly true in the case of polyacid and multivalent cations, where higher order complexes are involved in the ion condensation. Thus, in order to estimate the binding free energy for each type of complex (ANa, ACa^+, and A_2Ca), detailed molecular dynamic simulations, using different force fields and evaluating the obtained values in the light of previous computational and experimental[9-10] results, have been carried out in our lab. The corresponding results are available on arXiv.org (https://arxiv.org/abs/1801.05888).[11]

Effect of changing the electrolyte solution (from NaCl to KCl) on the conductance of the nanochannel.

In this work, we have studied the transport properties of PAA-functionalized nanochannels in NaCl solution due to its potential application in water desalination. However, in experiments, the ionic conductance of a nanochannel is often measured in KCl solution taking advantage of the fact that K^+ and Cl^- have similar diffusion coefficients.

In contrast to the experimental determination of the conductance of a nanochannel, our theoretical calculations do not require the use of ions with similar diffusion coefficients. Nevertheless, in order to address the qualitative differences between NaCl and KCl solutions, we recalculated here the information given in Figure 2 (Main Text), but this time using KCl instead

of NaCl. Figure S1 and S2 are comparison plots (NaCl vs. KCl) at $C_{Ca}^{2+} = 10^{-7}$ M and $C_{Ca}^{2+} = 10^{-2}$ M, respectively.

For these calculations, we took into account the size and diffusion coefficient of K^+ as well as the binding constant between K^+ and carboxylate ($-COO^-$):

- Molecular volume: $v_i = 0.011$ nm^3
- Diffusion coefficient: $D_i = 1.96 \times 10^{-9}$ m^2/s
- pK_d ($AK \rightleftharpoons A^- + K^+$) = -0.93

We based the later value on an educated guess. We took the binding constant calculated, by extensive MD simulations, for Na^+ in Ref.[11] as a reference value, and used the Na^+/K^+ binding ratio (with acetate ions) determined by Vrbka *et al.*[12] (i.e., 3.4) to estimate the dissociation constant for AK.

We first evaluate the effect of changing the electrolyte solution at very low calcium concentration, $C_{Ca}^{2+} = 10^{-7}$ M (Figure S1). Since the attractive interaction between K^+ and COO^- is weaker than the one between Na^+ and COO^-, a lower fraction of AK is formed (compare upper panels of Figure S1). In other words, under the same conditions, more deprotonated acidic groups are present inside the nanochannel in KCl solution than in NaCl solution. This produces a higher recruitment of potassium ions from the reservoirs and a higher presence of free K^+ inside the channel (middle panels of Figure S1), which consequently increases the total conductance of the channel (lower panels of Figure S1). In summary, at very low calcium concentration (Figure S1), only a small quantitative difference is observed in the gating properties of the nanochannel by changing the electrolyte solution from NaCl to KCl. In contrast, at $C_{Ca}^{2+} = 10^{-2}$ M (Figure S2), no appreciable difference is observed.

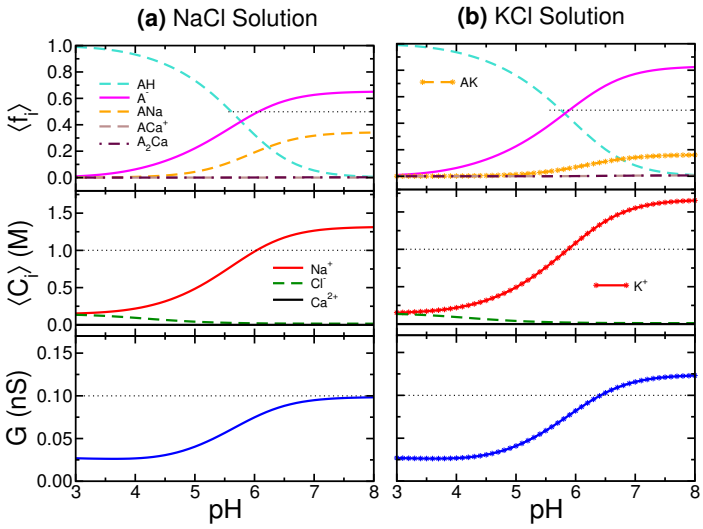

Figure S1. From top to bottom, pH dependence of: the average fraction of PAA segment states, $\langle f_i \rangle$; the average concentration of salt ions inside the channel, $\langle C_i \rangle$; and the nanochannel conductance, G. The parameters used for these calculations were exactly the same as in Figure 2a (Main Text), namely: R = 7.5, L = 12 μm, N = 45, σ = 0.1 chains/nm^2, and C_{Ca}^{2+} = 10^{-7} M. Calculations were made in different electrolyte solutions: (a) C_{NaCl} = 0.15 M and (b) C_{KCl} = 0.15 M.

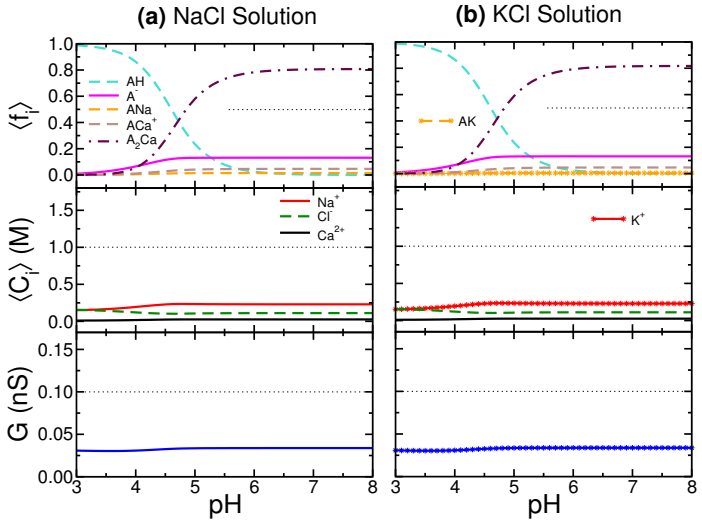

Figure S2. Same as in Figure S1, but at C_{Ca}^{2+} = 10^{-2} M. (a) C_{NaCl} = 0.15 M and (b) C_{KCl} = 0.15 M.

Effect of the grafting density, σ, on the conductance of the channel.

Complementing the results exposed in the Main Text, Figure S3 shows that the predicted conductance is highly dependent on the polymer grafting density, σ. At fixed values of N (polymer length) and R (radius), the grafting density is the only parameter that controls the number of PAA segments within the nanochannel. Thus, the larger the number of deprotonated segments, the greater the recruitment of counter ions, and, correspondingly, the higher the conductance of the nanochannel. These results agree with a previously reported linear dependence between the conductance and the factor σNR (namely, the number of polymer segments per unit length), that was observed for different combinations of σ, N, and R in a P4VP-modified nanochannel.[5]

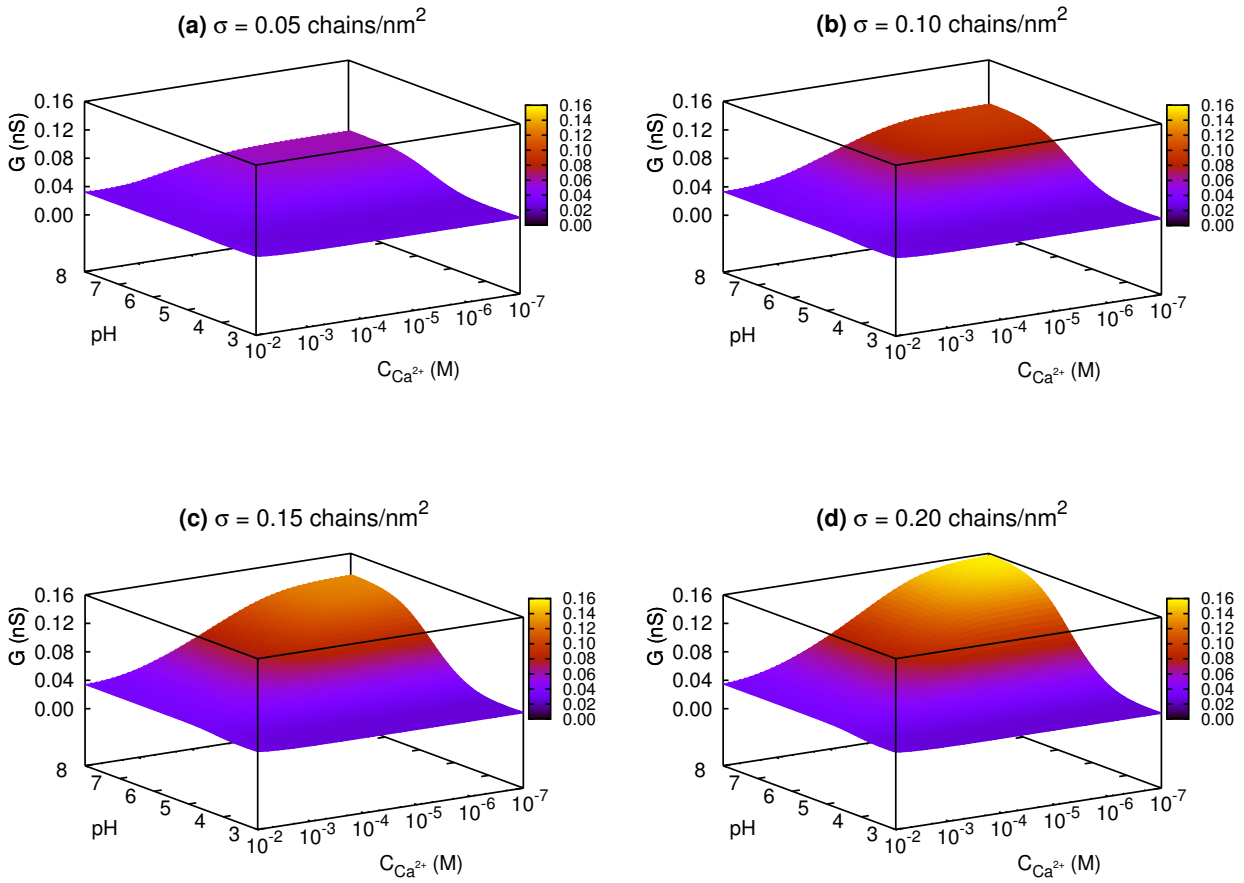

Figure S3. Nanochannel conductance, G, as a function of pH and calcium concentration, for different grafting densities, σ: (a) σ = 0.05 chains/nm^2, (b) σ = 0.10 chains/nm^2, (c) σ = 0.15 chains/nm^2, and (d) σ = 0.20 chains/nm^2. For all these plots, N = 45 and C_{NaCl} = 0.15 M.

Effect of NaCl concentration on the conductance of the nanochannel.

All the results presented in the Main Text have been calculated with a bulk NaCl concentration of 150 mM (physiological concentration). Here, we show the differences in the conductance of the channel and the thickness of the end-tethered polymer layer when a C_{NaCl} of 1mM, 10 mM, or 100 mM is used. As explained in the Main Text, Na^+ is the majority charge carrier within the channel. Figure S4 shows that a bulk NaCl concentration in the order of 10^{-1} M is needed in order to have a significant conductance in a nanochannel with the dimensions set for the present study.

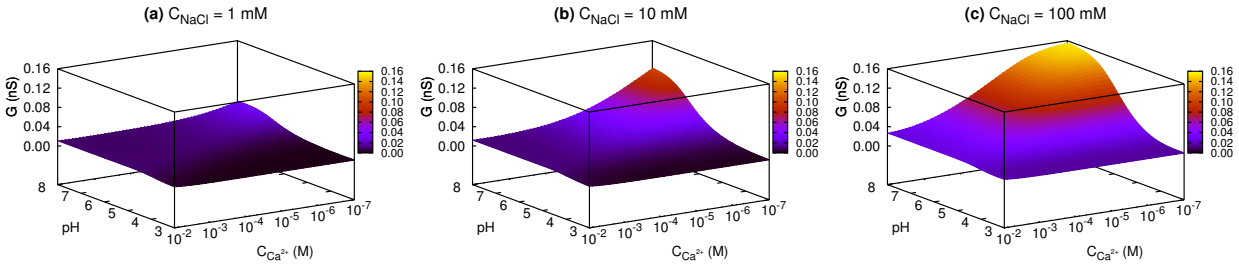

Figure S4. Conductance landscape as a function of pH and calcium concentration, C_{Ca}^{2+}. With the exception of NaCl concentration, the parameters are N = 45 and σ = 0.2 chains/nm^2, for the three plots. (a) C_{NaCl} = 1 mM, (b) C_{NaCl} = 10 mM, and (c) C_{NaCl} = 100 mM.

Variation of the electrostatic potential within the channel.

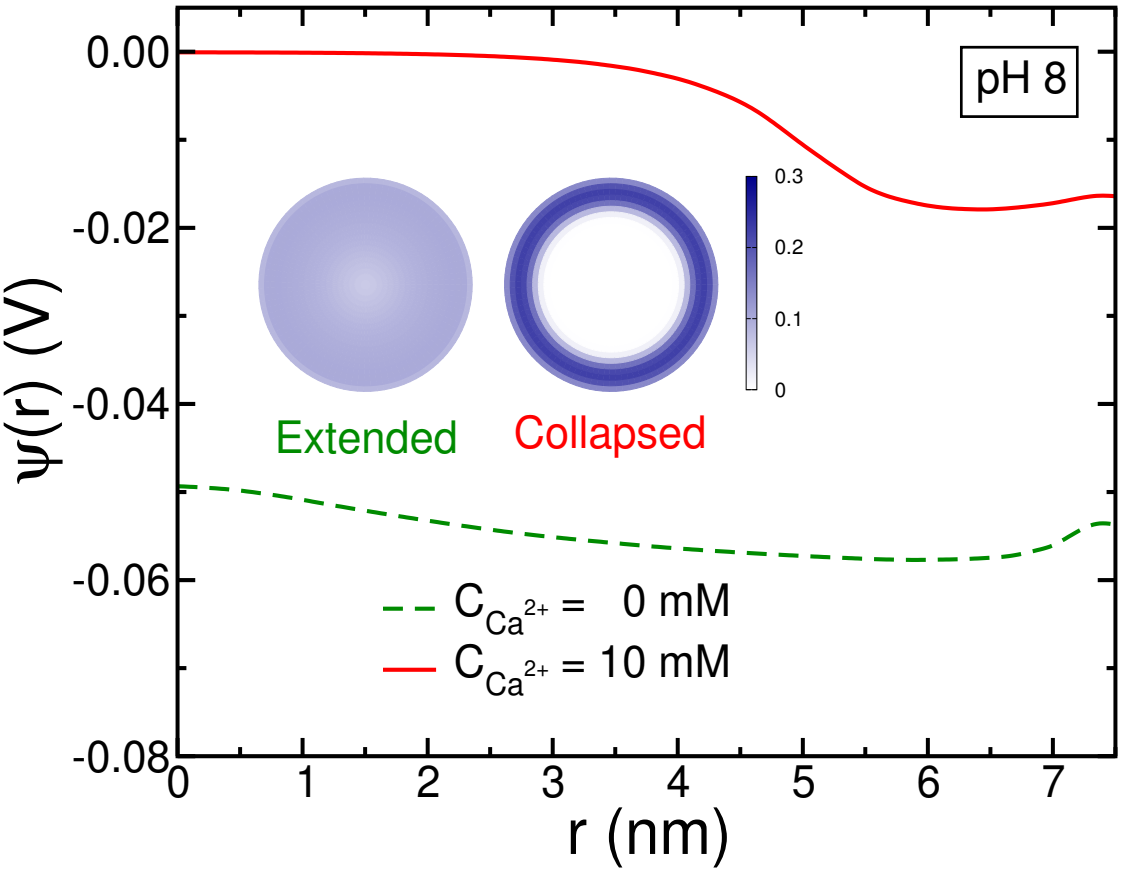

Figure S5. Electrostatic potential, $\psi(r)$, as a function of the distance, r, from the center of the channel (0 nm) to the wall (7.5 nm). The values of the parameters are the same as for Figure 4 (Main text). The green/dashed (red/solid) curve corresponds to the electrostatic potential curves in the absence (presence) of calcium ions. The inset shows the cross-sectional polymer volume fraction, $\langle \phi_p(r) \rangle$, of the nanochannel for both states.

Effect of the grafting density, σ, on the thickness of the end-tethered PAA layer, h.

Figure S6 shows that a more dramatic collapse of the end-tethered PAA layer on the nanochannel walls happens for lower grafting densities. This is an expected result. The more the space between chains, the greater the polymer contraction that can take place on the walls.

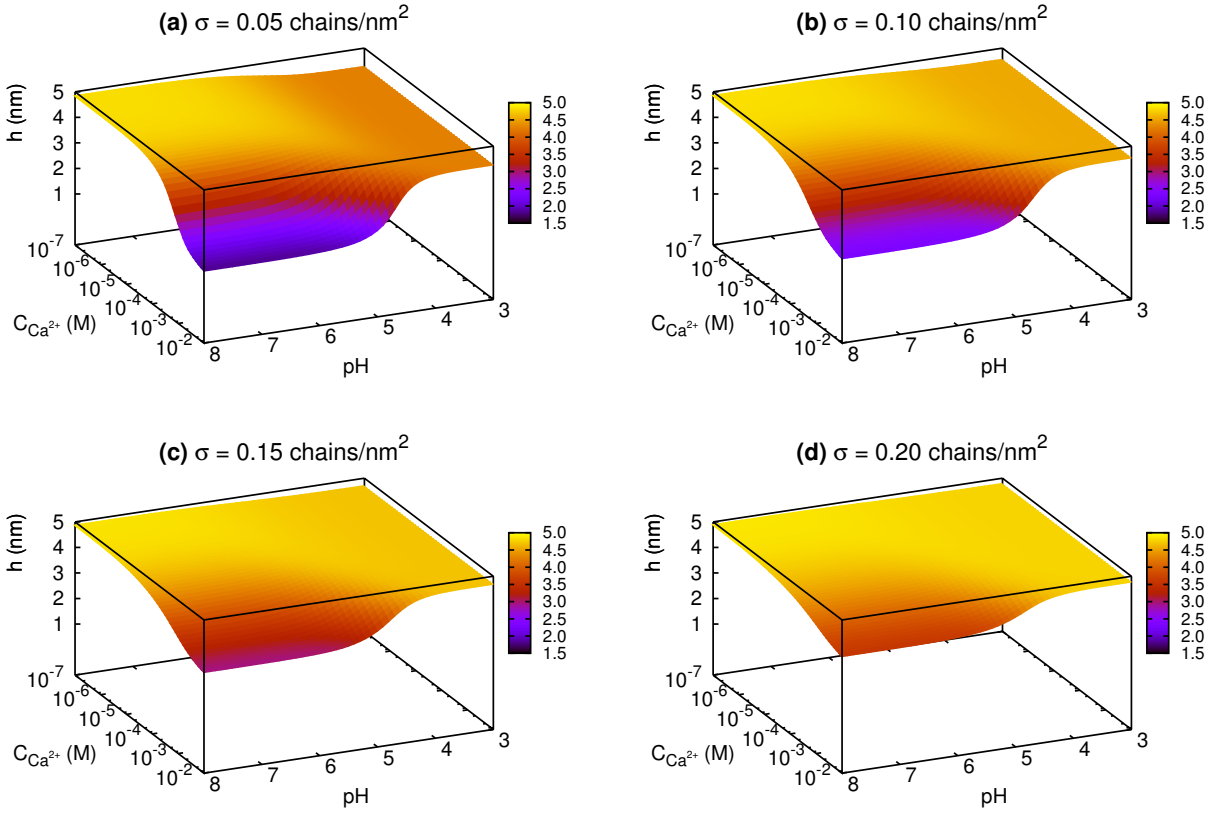

Figure S6. Thickness of the end-tethered PAA layer, h, as a function of pH and calcium concentration, for different grafting densities, σ: (a) σ = 0.05 chains/nm^2, (b) σ = 0.10 chains/nm^2, (c) σ = 0.15 chains/nm^2, and (d) σ = 0.20 chains/nm^2. For all these plots, N = 45 and C_{NaCl} = 0.15 M.

Effect of NaCl concentration on the thickness of the end-tethered PAA layer, h.

As can be seen in figure S7, at basic pH and low calcium concentrations (10^{-7}-10^{-4} M) the swelling of the chains is reduced when there is not enough Na^+ ions in the bulk solution. As it is explained in the Main Text of this paper, it is the uptake of counterions like Na^+ the factor that promotes the stretching of the charged polymer chains.

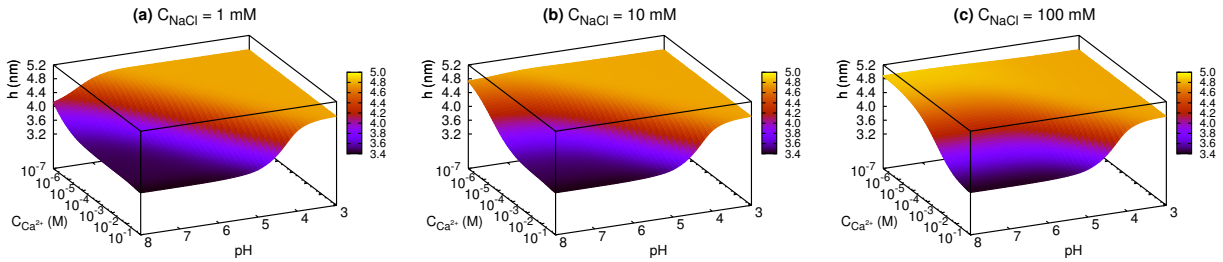

Figure S7. Landscape of the polymer layer thickness, h, as a function of pH and calcium concentration, C_{Ca}^{2+}. With the exception of the NaCl concentration value, the parameters are N = 45 and σ = 0.2 chains/nm^2, for the three plots. (a) C_{NaCl} = 1 mM, (b) C_{NaCl} = 10 mM, and (c) C_{NaCl} = 100 mM.

Interplay between polymer density and calcium binding.

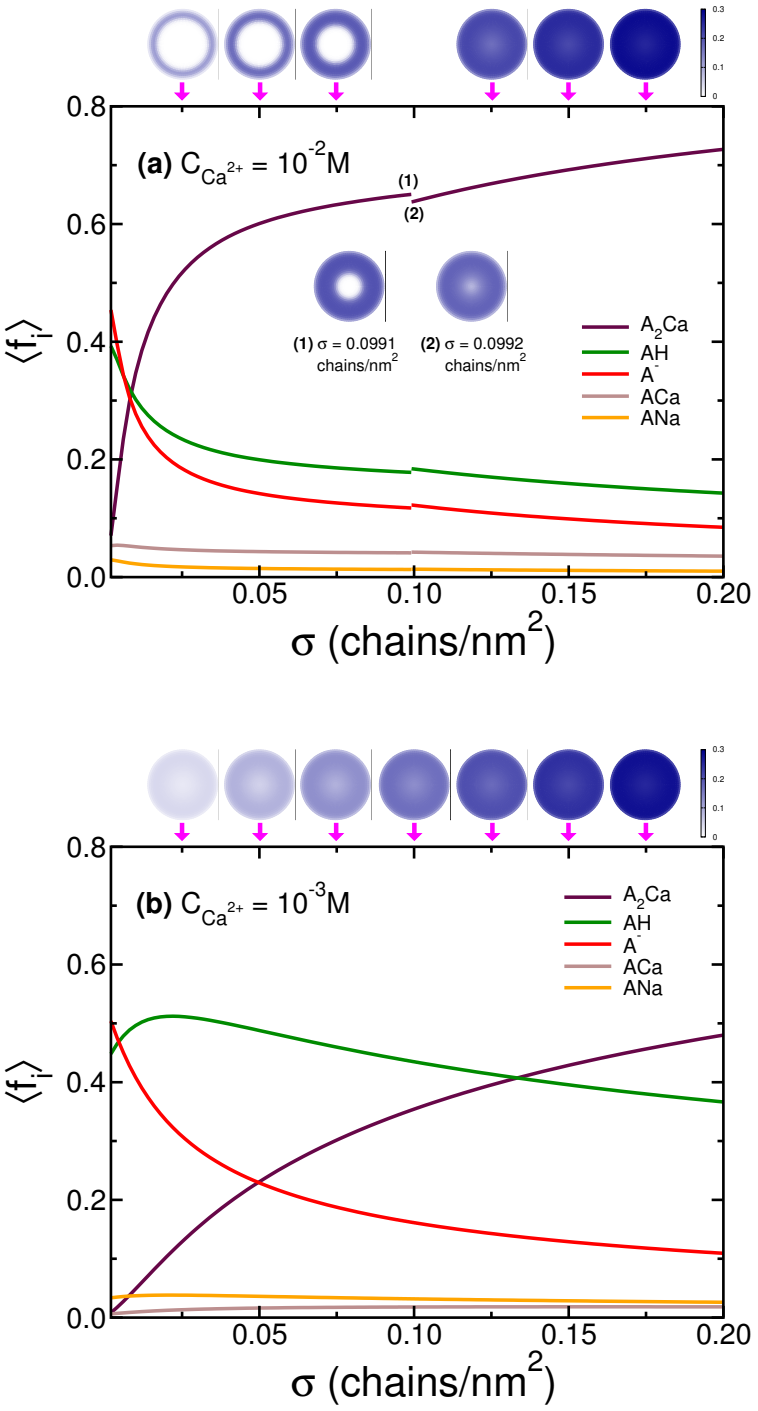

Figure S8. Effect of grafting density on the average fraction of protonated (AH), deprotonated (A^-), sodium and calcium bound poly(acrylic acid) segments. The parameters used for these calculations were: N = 75, pH 5.1, C_{NaCl} = 0.15 M, and C_{Ca}^{2+} = 0.01 M (a) or C_{Ca}^{2+} = 0.001 M (b).

Discontinuity in the nanochannel conductance.

A discontinuous behavior is also observed in the nanochannel conductance for intermediate-length chains (Figure S9). Although the magnitude of the conductance is low in this case, due to the presence of calcium ions in the system ($C_{Ca}^{2+} = 10^{-2}$ M), a clear difference can be noticed between the conductance of the center-phase and wall-phase configurations. As mentioned in the Theoretical Methodology section (Main Text), the expression used to calculate the conductance of the channel assumes that there is no fast exchange between bound and free counterions, and the diffusion coefficients of the ions are not affected by the polymer density. It is easy to see that a more realistic approximation (not developed here), which takes into account these effects, may lead to a higher conductance of the center-phase configuration (since the polymers are much less packed in this state than in the wall-collapsed state), thereby increasing the magnitude of the jump showed in Figure S9.

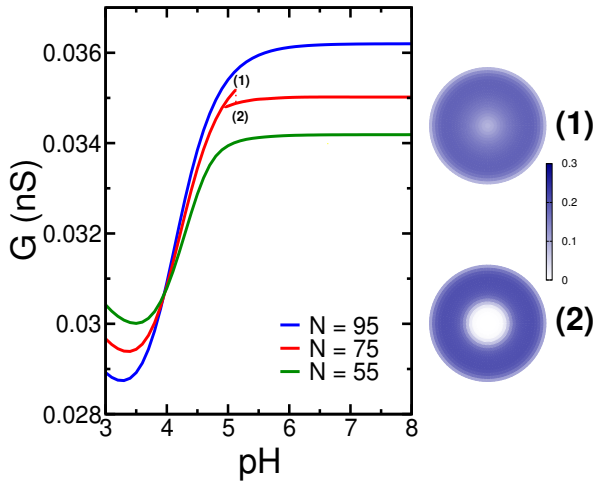

Figure S9. pH dependence of the conductance, *G*, for different polymer lengths. The conditions are exactly the same as in Figure 6 (see Main Text), and the channel length was set to 12 μm.

REFERENCES

1. Nap, R.; Gong, P.; Szleifer, I., Weak polyelectrolytes tethered to surfaces: Effect of geometry, acid-base equilibrium and electrical permittivity. *Journal of Polymer Science, Part B: Polymer Physics* **2006,** *44* (18), 2638-2662.
2. Vao-soongnern, V.; Merat, K.; Horpibulsuk, S., Interaction of the calcium ion with poly(acrylic acid) as investigated by a combination of molecular dynamics simulation and X-ray absorption spectroscopy. *Journal of Polymer Research* **2016,** *23* (1), 1-7.
3. Nap, R. J.; Park, S. H.; Szleifer, I., Competitive calcium ion binding to end-tethered weak polyelectrolytes. *Soft Matter* **2018,** *14* (12), 2365-2378.
4. Szleifer, I.; Carignano, M. A., Tethered polymer layers. In *Advances in Chemical Physics*, 1996; Vol. 94, pp 165-260.
5. Tagliazucchi, M.; Azzaroni, O.; Szleifer, I., Responsive polymers end-tethered in solid-state nanochannels: When nanoconfinement really matters. *Journal of the American Chemical Society* **2010,** *132* (35), 12404-12411.
6. Hindmarsh, A. C.; Brown, P. N.; Grant, K. E.; Lee, S. L.; Serban, R.; Shumaker, D. E.; Woodward, C. S., SUNDIALS: Suite of nonlinear and differential/algebraic equation solvers. *ACM Transactions on Mathematical Software* **2005,** *31* (3), 363-396.
7. Cussler, E. L., *Diffusion*. 2nd ed.; Cambridge University Press: 1997.
8. Haynes, W. M., *CRC Handbook of Chemistry and Physics*. 94th ed.; CRC Press: 2013.
9. Miyajima, T.; Mori, M.; Ishiguro, S. I., Analysis of complexation equilibria of polyacrylic acid by a Donnan-based concept. *Journal of Colloid and Interface Science* **1997,** *187* (1), 259-266.
10. Sinn, C. G.; Dimova, R.; Antonietti, M., Isothermal titration calorimetry of the polyelectrolyte/water interaction and binding of Ca2+: Effects determining the quality of polymeric scale inhibitors. *Macromolecules* **2004,** *37* (9), 3444-3450.
11. Park, S. H.; Nap, R. J.; Szleifer, I., Association Free Energies of Metal Cations with Mesylate and Acetate in Brine Calculated via Molecular Dynamics Simulation. *ArXiv e-prints* **2018**, arXiv:1801.05888[physics.chem–ph].
12. Vrbka, L.; Vondrášek, J.; Jagoda-Cwiklik, B.; Vácha, R.; Jungwirth, P., Quantification and rationalization of the higher affinity of sodium over potassium to protein surfaces. *Proceedings of the National Academy of Sciences* **2006,** *103* (42), 15440.